Computational Method for Crack Layer Model

Haiying Zhang[1,*], Alexander Chudnovsky[1]

[1] Department of Civil and Materials Engineering, University of Illinois at Chicago, 60607, USA
* Corresponding author: haiyin@uic.edu

Abstract Crack layer (CL) model is applied for modeling of brittle fracture of engineering thermoplastics. It specifically used in polyethylene structures, where a process zone (PZ) formed in front of crack is a narrow wage-type layer consisting of drawn fibers and membranes. To model CL requires an evaluation of stress intensity factors (SIF) and crack opening displacements (COD) within the crack and PZ domains. This paper is aimed to construct SIF and COD formulas for three specific geometries: a semi-infinite crack in an infinite solid; a single-edge notched specimen, standard Pennsylvania notch test (PENT, ASTM F 1473) and a new stiff constant-*K* (SCK) specimen. The approximate SIF and COD formulas are expressed as superposition of two elastic solutions one due to remote load and another associated with closing forces. The paper presents the computational technique in details. The approximate expressions of SIF and COD are used to present the method of computation the shape and the size of PZ, as well as the crack and PZ driving forces. The CL parameters then are used in simulation of CL growth and prediction of the lifetime of engineering structures made of thermoplastics.

Keywords Crack layer model, slow crack growth, process zone, Green's function

1. Introduction

In continuum mechanics, a crack is conventionally considered as an ideal cut in an elastic, elasto-plastic or visco-elasto-plastic medium. The concept of surface (fracture) energy associated with crack faces introduced by Griffith [1] was the first important step in thermodynamics of brittle failure. Barenblatt [2, 3] proposed a simple model of cohesive forces acting along the crack surfaces in a vicinity of crack tip. A year later Dugdale [4] independently developed a similar model for plastic deformation along an extension of crack-cut. Mathematically the two models turn to be identical and are commonly referred to as the Dugdale-Barenblatt (D-B) Model (also known as Cohesive Zone Model). The essential assumption of D-B model is that the stress singularity at the crack tip vanishes due to cohesive forces or plastic deformation at the crack front zone. Formally it expressed as zero stress intensity factor (SIF, K), i.e., $K = 0$. However, the stress singularity results from two basic assumptions of linear elastic fracture mechanics: 1) linear elastic stress-strain relations are maintained in near crack tip region without limitation; 2) the crack is ultimately sharp with zero curvature at the tip. In real engineering materials, however, neither of these two assumptions is correct. Indeed, 1) a damage in form of crazing, micro-cracking, shear-banding, cavitation etc. is formed in response to high stresses and the crack-damage interaction limits the stress level in the damage zone region; 2) large deformation of the crack front region results in the positive crack tip curvature, even when it could be zero before loading. It implies that the crack in engineering materials is commonly surrounded by a damage zone (generally called "process zone") and the crack-damage interaction plays the major role in formation of stress field as well as in fracture propagation process.

This leads to an alternative approach to studies of SCG known as Crack Layer (CL) model [5, 6]. CL model was originally proposed more than 3 decades ago and after that was further developed and applied for modeling various aspects of brittle fracture process [7-13]. In CL model the crack and the process zone, which usually precedes and surrounds the crack during fracture propagation in plastic components, considered as one thermodynamic system, Crack Layer. In HDPE, the process zone (PZ) is a thin wedge shape layer of cold drawn fibers and membranes. The stress and strain fields in CL model can be presented as a superposition of that in the specimen with cut off CL

subjected to an external load (F_∞ or σ_∞) and a thin wedge shape PZ domain with variable width ω_0 of original material that undergoes cold drawing under a distributed closing tractions σ_{dr} as shown in Figure 1.

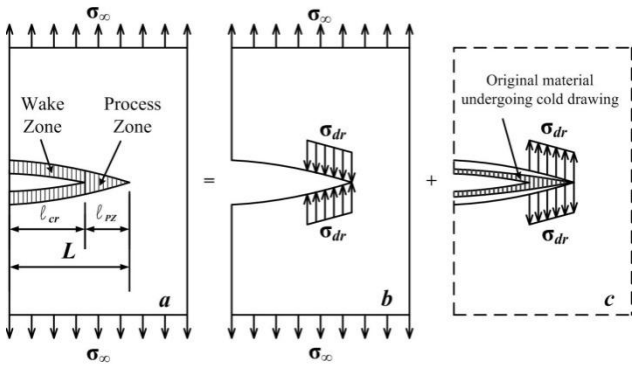

Figure 1. Decomposition of Crack Layer Model.

Accordingly, CL growth is decomposed into two closely coupled processes: 1) the PZ growth into the surrounding original material; 2) the crack penetration into the PZ [13].

The thermodynamic forces for such elementary processes are conventionally presented as the derivatives from Gibbs potential of the system with respect to the corresponding CL geometrical parameters such as the crack and the PZ lengths. Performing the calculations one can show that the thermodynamic force driving PZ growth X^{PZ} is expressed as [13]:

$$X^{PZ} = \frac{K_{tot}^2}{E'} - \gamma^{tr} \cdot \frac{\partial V^{PZ}}{\partial \ell_{PZ}}, \tag{1}$$

where K_{tot} is the total SIF presented as the sum of SIF due to remote load σ_∞ and SIF due to traction σ_{dr} along the PZ boundary; E' plane strain Young's modulus; γ^{tr} the specific energy of transformation, i.e., the work required to transform a unit mass of original material into an equal mass of oriented unstressed state plus the difference of strain energy densities in the original and drawn states; V^{PZ} PZ volume; and ℓ_{PZ} process zone size.

Similarly, the crack driving thermodynamic force X^{cr} has the following form [13],

$$X^{CR} = J_1^{cr} - 2\gamma, \tag{2}$$

where J_1^{cr} is the energy release rate due to crack extension into the PZ, when PZ is stationary, and 2γ is surface (fracture) energy per unit length.

A stationary CL configuration takes place, when the thermodynamic forces are not positive, i.e., $X^{PZ} \le 0$ and $X^{CR} \le 0$. The equilibrium is achieved, when the both forces equal zero. At a small deviation from equilibrium, a thermodynamic system has a tendency to return to the equilibrium state. However, fracture is an essentially irreversible process: there is no "healing", when the PZ fibers are broken, or PZ advances into the original material via cavitation followed by cold drawing of the material between the cavities and formation of membranes and fibers. Thus, when CL departs from one stationary state, it moves into next stationary configuration. Such process of crack layer propagation continues by crack and process zone assisting mutual growth. The described CL propagation is formalized in the following system of coupled ordinary differential equations with respect to the crack length (ℓ_{cr}) and the PZ size (ℓ_{pz}):

$$\begin{cases} \dot{\ell}_{cr} = k_1 X^{CR}, \ if \ X^{CR} \geq 0, and \ \dot{\ell}_{cr} = 0, if \ X^{CR} < 0 \\ \dot{\ell}_{pz} = k_2 X^{PZ}, \ if \ X^{PZ} \geq 0, and \ \dot{\ell}_{pz} = 0, if \ X^{PZ} < 0 \end{cases}, \tag{3}$$

where k_1, and k_2 are the kinetic coefficients, which are evaluated experimentally.

Evaluation of CL driving forces requires a computation of SIF and crack opening displacement (COD). In this paper we present a semi-analytical method of SIF and COD computations. The method is illustrated by solution for three geometries: a semi-infinite crack in an infinite solid; a single-edge notched specimen, standard PENT specimen (ASTM F 1473) and a stiff constant-*K* (SCK) specimen. The approximate formulas for SIF and COD are expressed as superposition of two elastic solutions for the listed above samples due to: 1) remote load σ_∞ or F_∞ ; and 2) closing force σ_{dr}. The close form solution for a semi-infinite crack in an infinite homogeneous and linear elastic solid is used as the basic expression. The solution for any finite specimen geometry is constructed by introducing a geometry correction factor to the basic expression. The Green's functions technique is effectively used to construct analytical expressions for SIF and COD. Then, the approximate expressions for SIF and COD are employed in computations of the CL driving forces and simulations of the slow fracture propagation process in HDPE [8, 13].

2. Semi-Infinite Crack in an Infinite Plate

2.1. SIF Formula

The decomposition shown in Fig. 1 is first applied to the semi-infinite crack in an infinite homogeneous and linear elastic solid subjected to a distributed load σ_∞ over L and a crack closing load σ_{dr} on PZ (see Figure 2 below). L is the length of CL, which is the summ of actual crack length ℓ_{cr} and PZ size ℓ_{pz}, i.e., $L = \ell_{cr} + \ell_{pz}$. The SIF Green's function for the semi-infinite crack is well known:

$$G^{SIF}(x) = \sqrt{\frac{2}{\pi x}}, \tag{4}$$

where the origin of the coordinates is placed at the crack tip.

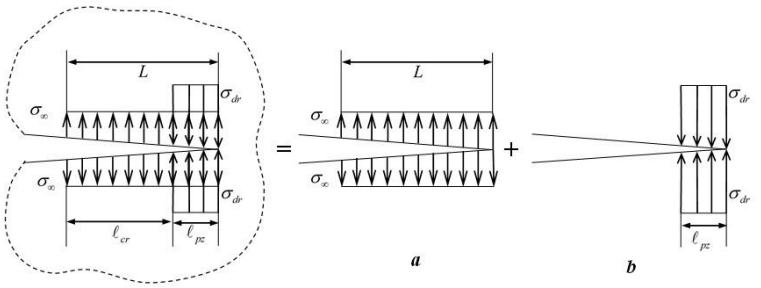

Figure 2. Decomposition of the problem of a semi-infinite crack in an infinite plate subjected to a distributed load σ_∞ and a closing force σ_{dr} on PZ.

For the boundary conditions and loading shown in Figure 2 *a* and *b*, SIFs are readily obtained by the standard application of Green's function:

Boundary Condition *a*: $$K_\infty = K_I(\sigma_\infty) = \int_0^L \sigma_\infty G^{SIF}(x)dx = \frac{2\sqrt{2}\sigma_\infty\sqrt{L}}{\sqrt{\pi}} \ ; \tag{5}$$

Boundary Condition *b*: $$K_{dr} = K_I(\sigma_{dr}) = \int_0^{\ell_{pz}} \sigma_{dr} G^{SIF}(x)dx = \frac{2\sqrt{2}\sigma_{dr}\sqrt{\ell_{pz}}}{\sqrt{\pi}} \quad . \tag{6}$$

By applying the superposition to stress filed, the total SIF for the semi-infinite crack loaded as shown on the left side of Figure 2 is:

$$K_{tot} = K_\infty - K_{dr} = \frac{2\sqrt{2}}{\sqrt{\pi}}\left(\sigma_\infty\sqrt{L} - \sigma_{dr}\sqrt{\ell_{pz}}\right) \quad . \tag{7}$$

2.2. COD Formula

The COD $\delta(x)$ is convenient to express in the following integral form using an axillary fictitious force $Q(x)$ perpendicular crack face [14]:

$$\delta(x) = \frac{2}{E'}\int_0^L K_I(\sigma_\infty,\xi)K_I(Q,\xi)\Big|_{Q=1} d\xi \quad . \tag{8}$$

We select the origin of coordinate at the beginning of distributed load σ_∞, i.e., on the distance L from the crack tip (see Figure 2a). For calculations of COD δ due to distributed load two cases should be considered: **Case I**: $0 < x \le L$, $x \le \xi \le L$ and **Case II**: $x \le 0$, $0 \le \xi \le L$.

In the Case I,

$$\delta(\sigma_\infty, x) = \frac{2}{E'}\int_x^L \left[K_I(\sigma_\infty,\xi)K_I(Q,\xi)\right]\Big|_{Q=1} d\xi \tag{9}$$

Substituting Eqs. 4 and 5 into Eq. 9, one can find the COD formula. It is noted that x in Eq. 4 should be replaced by $\xi - x$ due to the change of the origin. Finally, the COD is:

Case I: $\delta(\sigma_\infty, x) = \frac{8\sigma_\infty}{\pi E'}\int_x^L \frac{\sqrt{\xi}}{\sqrt{\xi - x}} d\xi$; and Case II: $\delta(\sigma_\infty, x) = \frac{8\sigma_\infty}{\pi E'}\int_0^L \frac{\sqrt{\xi}}{\sqrt{\xi - x}} d\xi$ (10)

Performing the integration in (10), and shifting the origin to the crack tip one finds the COD:

$$\delta_\infty = \delta(\sigma_\infty, x) = \frac{8\sigma_\infty}{\pi E'}\sqrt{Lx} + \frac{4\sigma_\infty(L-x)}{\pi E'}\ln\left|\frac{\sqrt{x}+\sqrt{L}}{\sqrt{x}-\sqrt{L}}\right|, \quad x \ge 0 . \tag{11}$$

The reduction of COD due to the closing force σ_{dr} is determined by the same procedure. It takes form:

$$\delta_{dr} = \delta(\sigma_{dr}, x) = \frac{8\sigma_{dr}}{\pi E'}\sqrt{\ell_{pz}x} + \frac{4\sigma_{dr}(\ell_{pz}-x)}{\pi E'}\ln\left|\frac{\sqrt{x}+\sqrt{\ell_{pz}}}{\sqrt{x}-\sqrt{\ell_{pz}}}\right|, \quad x \ge 0 . \tag{12}$$

The analytical expression for total COD for the semi-infinite crack loaded as shown in Fig.2 is:

$$\begin{aligned}\delta_{tot}(x) = \delta(\sigma_\infty, x) - \delta(\sigma_{dr}, x) &= \frac{8\sigma_\infty}{\pi E'}\sqrt{Lx} + \frac{4\sigma_\infty(L-x)}{\pi E'}\ln\left|\frac{\sqrt{x}+\sqrt{L}}{\sqrt{x}-\sqrt{L}}\right| \\ &- \frac{8\sigma_{dr}}{\pi E'}\sqrt{\ell_{pz}x} - \frac{4\sigma_{dr}(\ell_{pz}-x)}{\pi E'}\ln\left|\frac{\sqrt{x}+\sqrt{\ell_{pz}}}{\sqrt{x}-\sqrt{\ell_{pz}}}\right|\end{aligned} \quad . \tag{13}$$

Figure 3 shows an example of COD profile for normalized stress $\bar{\sigma} = \sigma_\infty/\sigma_{dr} = 0.4$ and CL sizes

$\bar{\ell}_{pz} = \ell_{pz}/\ell_{cr} = 0.1$. Clearly the COD formula captures the beak-type opening at the tip of the crack.

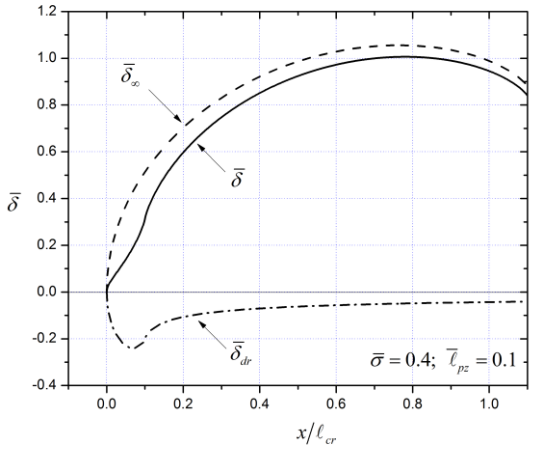

Figure 3. A COD in the crack – load configuration shown in Figure 2 left. Dashed line is COD due to $\bar{\sigma} = 0.4$; the negative COD is the closure due to drawing stress $\bar{\ell}_{pz} = 0.1$.

3. Single Edge Notch Specimen

The PENT is a standard test widely used for evaluation of the slow crack growth (SCG) resistance of polyethylene (PE) pipes. In PENT the failure time is recorded and used to rank various PE with respect to SCG resistance.

3.1. SIF Formula

A single edge notch (SEN) specimen is used in PENT. The specimen is subjected to a constant load ($\sigma_\infty = 2.4MPa$) and undergoes creep until failure. A closing load σ_{dr} is applied on the PZ that is in front of actual crack. The SIF due to σ_∞ is determined in the following way [14]:

$$K_\infty = K_I(\sigma_\infty) = \sigma_\infty \sqrt{\pi L} \cdot F_1(L/W). \tag{14}$$

where, L is CL length ($L = \ell_{cr} + \ell_{pz}$) in mm, W the width of the specimen in mm. The correction factor $F_1(L/W)$ with better than 0.5% accuracy can be found in [14].

Similarly the SIF Green's function for SEN specimen is (x is counted from the edge) is:

$$G_{SEN}^{SIF} = \frac{2}{\sqrt{\pi L}} \cdot F_2(x/L, L/W), \tag{15}$$

with the correction factor $F_2(L/W)$ given in [14]. Thus, $K_{dr} = \int_{\ell_{cr}}^{L} \frac{2\sigma_{dr}}{\sqrt{\pi a}} \cdot F_2(x/L, L/W)\,dx$ and by superposition one readily finds the total SIF expression in terms of known correction factors:

$$K_{tot} = \sigma_\infty \sqrt{\pi L} \cdot F_1(L/W) - \int_{\ell_{cr}}^{L} \frac{2\sigma_{dr}}{\sqrt{\pi L}} \cdot F_2(x/L, L/W)\,dx. \tag{16}$$

3.2. COD Formula

The COD depends on the crack size ℓ_{cr}, the PZ size ℓ_{pz}, the width of the specimen W, and the load. It is convenient to normalize the crack size and PZ size as follows $\overline{\ell}_{cr} = \ell_{cr}/W$ and $\overline{\ell}_{pz} = \ell_{pz}/\ell_{cr}$. The COD for PENT specimen has been evaluated numerically using FRANC2D. The calculation has been carried on a series of PENT specimen configurations with $\overline{\ell}_{cr} = 0.35, 0.45, 0.55$. For each $\overline{\ell}_{cr}$, the normalized PZ size varies $\overline{\ell}_{pz} = 0.1, 0.2, 0.3, 0.4$. By comparing the numerical results with COD for the semi-infinite crack, we obtain the COD expression for the PENT. Here "comparison" means the first term on the right hand side of semi-infinite crack solution (Eq. 11) is replaced by the Williams expansion [15] $\left(ax^{1/2} + bx^{3/2} + cx^{5/2} + ...\right)$, x is the distance measured from the tip of the PZ, and the higher order term are ignored. The difference is represented by $Diff$ throughout the paper. The coefficients a, b, and c are determined for each combination of $\overline{\ell}_{cr}$ and $\overline{\ell}_{pz}$ by least squares fitting. Analytical expressions for three coefficients are provided by fitting the numerical results.

Hence, the normalized COD due to the remote load σ_∞ is the sum of $Diff$ and the second term in the right hand side of the semi-infinite crack solution (Eq. 11):

$$\delta_\infty = \delta(\sigma_\infty, \overline{x}) = \frac{8\sigma_\infty W}{\pi E'}\left[\sqrt{\overline{x}}\left(a + b\overline{x} + c\overline{x}^2\right) + \frac{1}{2}\overline{\ell}_{cr}\left(1 + \overline{\ell}_{pz} - \overline{\ell}_{pz}\overline{x}\right)\ln\left|\frac{\sqrt{\overline{\ell}_{pz}\overline{x}} + \sqrt{1+\overline{\ell}_{pz}}}{\sqrt{\overline{\ell}_{pz}\overline{x}} - \sqrt{1+\overline{\ell}_{pz}}}\right|\right]. \tag{17}$$

The same procedure is applied to the COD due to σ_{dr}, except that the second term on the right hand of Eq. 12 instead of Eq. 11 is used. It leads to the following expressed:

$$\delta_{dr} = \delta(\sigma_{dr}, \overline{x}) = \frac{8\sigma_{dr} W}{\pi E'}\left[\sqrt{\overline{x}}\left(a' + b'\,\overline{x} + c'\,\overline{x}^2\right) + \frac{1}{2}\overline{\ell}_{cr}\,\overline{\ell}_{pz}\left(1 - \overline{x}\right)\ln\left|\frac{\sqrt{\overline{x}}+1}{\sqrt{\overline{x}}-1}\right|\right]. \tag{18}$$

The total opening δ_{tot} is: $\delta_{tot} = \delta_\infty - \delta_{dr}$.

4. Constant-*K* Specimen

Equation of SCG is commonly formulated as a functional relation between crack growth rate and SIF that usually depends on the remote load, crack and PZ lengths (CL size) as well as specimen geometry. Thus, one needs to monitor crack and PZ lengths in real time to formulate CL growth equations. It is technically challenging to monitor CL dimensions in SCG process in not transparent materials. A specimen for which SIF does not depend on crack length allows one to reconstruct the SCG rate ~ SIF relations without monitoring the process. Tapered Double Cantilever Beam (TDCB) has long been used for crack growth studies in metals [16]. Unfortunately, in application to polymers, TDCB specimen displays a very large deformation that compromises the assumptions of linear elasticity. A stiff constant-*K* (SCK) specimen has been design for relatively soft materials [13]. It is stiffer than TDCB and a few other alternative specimen geometries examined. That was a reason for the name. The diameters and locations of holes are designed to maintain the constancy of SIF. The side grooves reduce the plane stress effect in the surface layers.

4.1. SIF Formula

In SCK specimen, SIF due to remote load F_∞ is independent on crack length in the crack size range $0.15 < \ell_{cr}/W < 0.4$ and simply related to the applied load (F_∞, B_0, B_e, and W are specified in Figure 5):

$$K_\infty \equiv K_I\left(F_\infty\right) = 6.56\frac{F_\infty}{B_{eff}\sqrt{W}}. \tag{19}$$

The Green's function for SIF due to self-equilibrated double forces applied to the crack faces in SCK specimen is obtained by introducing a correction factor to the Green's function of semi-infinite crack in an infinite solid ($G^{semi} = \sqrt{\frac{2}{\pi x}}$):

$$G^{SCK}(x,L,W) = \sqrt{\frac{2}{\pi x}} + \frac{\alpha}{L}x^{1/2} + \frac{\beta}{L^2}x^{3/2}. \tag{20}$$

where x is the distance from the tip of crack layer (CL), L is CL length ($L = \ell_{cr} + \ell_{pz}$)
Thus, the SIF due to σ_{dr} is obtained by integrating the Green's function over the PZ size and the total SIF K_{tot} is obtained by $K_{tot} = K_\infty - K_{dr}$.

4.2. COD Formula

Based on numerical analysis of SCK specimens with different geometries ($\ell_{pz}/L = 0.1$, 0.2, 0.25, 0.3; and $L/W = 0.2$, 0.25, 0.3, 0.35), the COD δ_∞ and δ_{dr} at a point x due to the remote load F_∞ and σ_{dr} respectively can be presented in the following forms:

$$\delta_\infty = \frac{8}{\pi E'}\frac{F_\infty}{\sqrt{B_0 B_e}}\sqrt{\frac{x}{L}}\left(\alpha + \beta\frac{x}{L} + \gamma\frac{x^2}{L^2}\right) \text{ and } \delta_{dr} = \frac{8\sigma_{dr}W}{\pi E'}\sqrt{\frac{x}{\ell_{pz}}}\left(\alpha' + \beta'\frac{x}{\ell_{pz}} + \gamma'\frac{x^2}{\ell_{pz}^2}\right) \tag{21}$$

The coefficients α, β, and γ are functions of only one variable L/W and the coefficients α', β', and γ' are simple functions of ℓ_{pz}, L and W. The total opening is: $\delta_{tot} = \delta_\infty - \delta_{dr}$.

The same approach is readily applicable to other specimen geometries. Thus, the evaluation of CL parameters is the building block for calculation of CL driving forces and simulation of CL growth.

5. Examples of Crack Layer Growth Simulation

The process zone driving force X^{PZ} monotonically decreases with increase of PZ size. The equilibrium PZ size ℓ_{pz}^{eq} corresponds to vanishing of the corresponding thermodynamic force:

$$\frac{K_{tot}^2}{E'} - \gamma^{tr}\cdot\left.\frac{\partial V^{PZ}}{\partial \ell_{PZ}}\right|_{x=\ell_{pz}} = 0. \tag{22}$$

The experimental determination of the equilibrium PZ size is conducted by direct observations of striations of fracture surface in discontinuous CL growth. A comparison of calculated equilibrium PZ size ℓ_{pz}^{eq} with experimental data (Figure 4 (a)) at elevated temperature is shown in Figure 4 (b).

Note the experimental equilibrium size of process zone is measured directly from the fracture surface as shown in Figure 4 (a). The CL model predictions agree very well with observations. It is also interesting to compare ℓ_{pz}^{eq} with conventional D-B model prediction. The process zone size ℓ_{pz}^{DB} in D-B model is determined by the requirement $K_{tot}=0$ with K_{tot} defined by $K_{tot}=K_{\infty}-K_{dr}$. It is also shown in Figure 4 (b) that the experimentally observed equilibrium size of process zone ℓ_{pz}^{eq} is significantly smaller than ℓ_{pz}^{DB} predicted by D-B model. In this specific example, the equilibrium size of process zone ℓ_{pz}^{eq} is within the range of 1.3~2.8mm, whereas D-B prediction ℓ_{pz}^{DB} is between 3.8~8.8mm, three times larger. This could be expected since the D-B model ignores the energy dissipation by cold drawing of original material into the oriented fibers of PZ. There are clear trends in ℓ_{pz}^{eq} dependency on load and temperature: 1) For a given temperature, the equilibrium PZ size ℓ_{pz}^{eq} linearly increases with increase of load; 2) For the same value of K_{∞}, ℓ_{pz}^{eq} increases with increase of temperature; 3) The ℓ_{pz}^{eq} in CL model is significantly smaller than the D-B zone size; 4) The difference between the equilibrium PZ in CL and D-B zone sizes increases with increasing load.

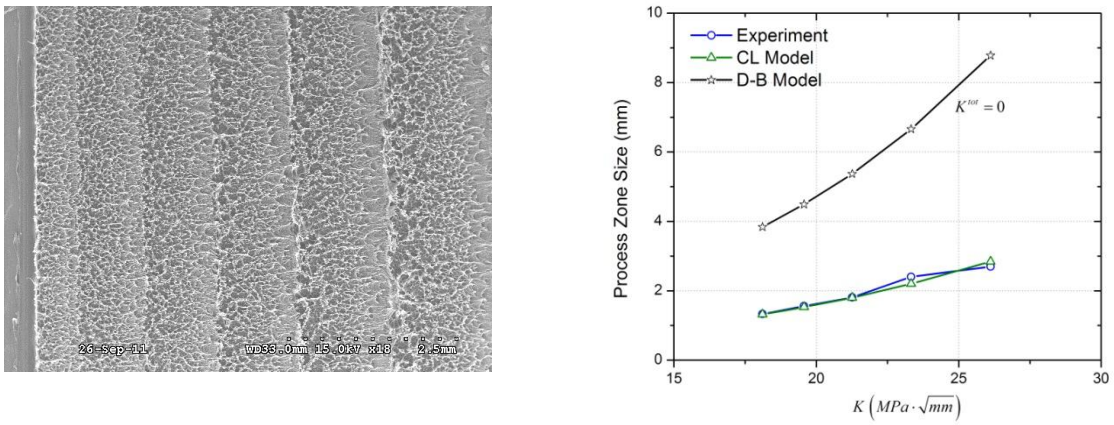

(a) (b)

Figure 4. (a). Fracture surface of a CT specimen test at 80°C (Note: the first striation is resulted from the pre load and thus ignored); (b) Comparison of predicted ℓ_{pz}^{eq} values with observations from (a).

The PZ and crack thermodynamic forces (Eqs. 1-2) are non-linear functions of crack and process zone lengths. Thus, the system of Eq. 3 despite of its simple appearance is a nonlinear system of ODE, solution of which calls for numerical methods. Below we show two examples of numerical simulation of CL growth in a compact tension (CT) specimen that has the same geometry as SCK except holes. SIF in CT specimen increases with crack length. The first example is shown in Figures 5 (a). It presents a discontinuous, stepwise crack layer growth from one stationary CL configuration to the next one.

At the beginning the crack is stationary, whereas PZ grows toward its equilibrium size $L \approx 9.5mm$. The first equilibrium size of CL L is reached in about $t=4\,hours$, and is maintained constant until the degradation of PZ material triggers the crack growth into PZ. It is depicted by the lower dash line moving up at $t\approx 28\,hours$. The crack propagates through PZ and gets arrested at the time $t\approx 33\,hours$, when it meets the original material at the tip of PZ. PZ grows accompanying the crack growth, since $X^{PZ}>0$ during this time; X^{PZ} decreases with an increase of the PZ length and CL

reaches the second stationary configuration, when X^{PZ} vanishes. A newly drawn material constitutes the new PZ. Then, the same degradation process takes over the drawn material and crack propagates through the second PZ the same way as in the first step. In CT specimen, the maximal value of X^{PZ} increases with CL length. As a result, the equilibrium PZ size increases and the duration of steps decreases with step number leading to an accelerated CL growth and final instability and transition to rapid crack propagation.

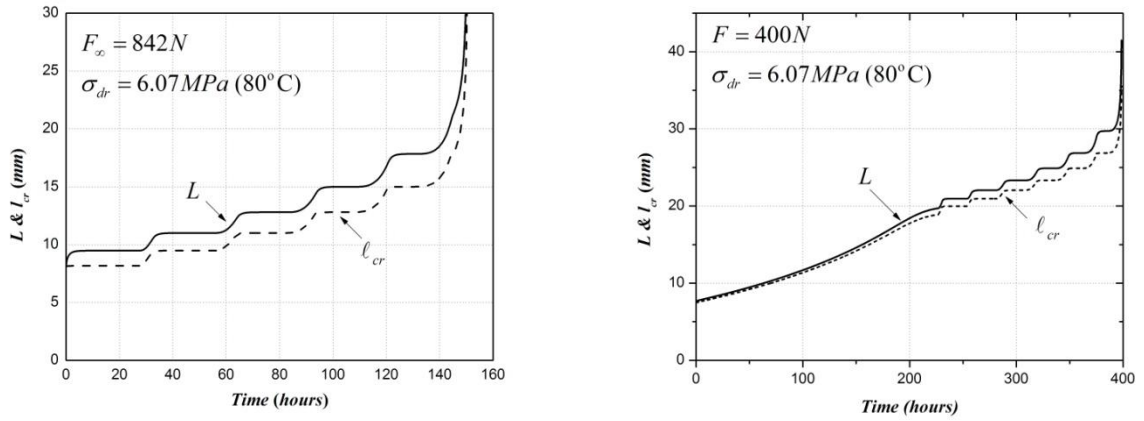

(a) (b)

Figure 5. (a) Numerical simulation of discontinuous crack layer growth for a CT specimen at 80°C; (b) Numerical simulation of transition from continuous to discontinuous CL growth.

The second example presents a different scenario of CL propagation: a transition from continuous to a discontinuous, stepwise CL growth shown in Figure 5 (b).

In this case, at the beginning, the PZ material degradation rate is comparable with the rate of PZ growth. In such case, the crack starts to grow into PZ before PZ reaches equilibrium. This process appears as continuous CL growth and the lines of $\ell_{cr}(t)$ and $L(t)$ practically coincide up to $t \approx 33\,hours$ as shown in Figure 5 (b). However, with increase of K_{tot} the PZ growth rate increases whereas the degradation rate of PZ material is the same. Thus, PZ "runs" away from the crack and PZ size becomes larger and larger and finally reaches the equilibrium size. It triggers a transition of from continuous CL growth mechanism to the discontinuous one. After such transition, the same process of discontinuous CL growth as described above (Figure 5 (a)) takes place.

For comparison with the vast literature on phenomenological crack growth studies, we introduce an average rate of crack layer growth $<\dot{L}>$ as a ratio between CL length increment in discontinuous growth and the duration of corresponding step. A correspondence between $<\dot{L}>$ and the SIF due to remote load K_∞ in double logarithmic scale represents the crack layer growth simulation in the conventional Paris-Erdogan equation form. The rate $<\dot{L}>$ depends on basic fracture parameters such as kinetic coefficients k_1 and k_2 in Eq. 3, σ_{dr}, γ^{tr} and γ as well as elastic and creep properties. It also depends on specimen shape and size, crack size as well as the magnitude and rate of applied load. The relation between the numerical simulation of $<\dot{L}>$ and the remote load SIF K_∞ allows one to establish a correspondence between empirical coefficients in Paris-Erdogan equation and basic material properties. Apparently, there are changes in the SCG pattern depending on load, CL size and temperature. It can be translated into different powers in Paris-Erdogan equation.

6. Conclusions

The focus of the paper is brittle fracture in PE structures resulting from crack growth. We outlined an alternative to the conventional approach for lifetime assessment. Our approach consists of a sound physical model of SCG and numerical simulation of the process. A combination of modeling and experimental work is required to evaluate the basic parameters employed in constitutive equations of the model. After that the numerical simulation of SCG can be readily performed. The experimental work is convenient to conduct with SCK specimen, since no in-situe observation is required and numerical tools for data analysis are developed. Note: the crack initiation time is ignored. Thus, the lifetime assessment is a conservative one: it gives the lower bound of life expectance.

References

[1] A.A. Griffith, The phenomena of rupture and flow in solids. Philos T Roy Soc A, 221 (1921) 163–198.
[2] G.I. Barenblatt, On equilibrium cracks formed in brittle fracture. General concepts and hypothesis. Axisymmetric cracks. J Appl Math Mech (PPM), 23, No. 3 (1959) 622–636.
[3] G.I. Barenblatt, Mathematical theory of equilibrium cracks in brittle fracture, Adv Appl Mech, VII (1962) 55–129.
[4] D.S. Dugdale, Yielding of steel sheets containing slits. J Mech Phys Solids, 8 (1960) 100–104.
[5] A. Chudnovsky, V.A. Dunaevsky, and V.A. Khandogin, On the Quasistatic Growth of Cracks, Arch Mech, 30, 2 (1978) 165–174.
[6] V. Khandogin, A. Chudnovsky, The Thermodynamic Analysis of Quasistatic Crack Growth, Dynamics and Strength of Aircraft Construction, 4 (1978) 148–175.
[7] J. Botsis, A. Chudnovsky, A. Moet, Fatigue Crack Layer Propagation in Polystyrene. 1. Experimental-Observations, Int J Fracture, 33 (1987) 263–276.
[8] J. Botsis, A. Chudnovsky, A. Moet, Fatigue Crack Layer Propagation in Polystyrene. 2. Analysis, Int J Fracture, 33 (1987) 277–284.
[9] K. Kadota, A. Chudnovsky, Constitutive-Equations of Crack Layer Growth, Polym Eng Sci, 32 (1992) 1097–1104.
[10] A. Stojimirovic, K. Kadota, A. Chudnovsky, An Equilibrial Process Zone in Polymeric Materials, J Appl Polym Sci, 46 (1992) 1051–1056.
[11] B. H. Choi, W. Balika, A. Chudnovsky, G. Pinter, R.W. Lang, The Use of Crack Layer Theory to Predict the Lifetime of the Fatigue Crack Growth of High Density Polyethylene, Polym Eng Sci, 49 (2009) 1421–1428.
[12] A. Chudnovsky, Y. Shulkin, Application of crack layer theory to modeling of slow crack growth in polyethylene, Int J Fracture, 97 (1999) 83–102.
[13] A. Chudnovsky, Z. Zhou, and H. Zhang, Lifetime Assessment of Engineering Thermoplastics, Int J Eng Sci, 59 (2012) 108–139.
[14] H. Tada, P. Paris, and G. Irwin, The Stress Analysis of Crack Handbook, ASME Press, New York, 2000.
[15] M.L. Williams, On the stress distribution at the base of a stationary crack, J Appl Mech, 24 (1957) 109–114.
[16] S. Mostovoy, P.B. Crosley, and E.J. Ripling, Use of crack loaded specimens for measuring plane-strain fracture toughness, J Mater, 2 (1967) 661–681.